A new method of spike modelling and interval analysis

Title: A New Method of Spike Modelling and Interval Analysis

Authors: D.J. MacGregor, C.K.I. Williams, G. Leng

PII: S0165-0270(08)00460-3
DOI: doi:10.1016/j.jneumeth.2008.08.011
Reference: NSM 5003

To appear in: *Journal of Neuroscience Methods*

Received date: 23-4-2008
Revised date: 1-8-2008
Accepted date: 5-8-2008

Please cite this article as: MacGregor DJ, Williams CKI, Leng G, A New Method of Spike Modelling and Interval Analysis, *Journal of Neuroscience Methods* (2007), doi:10.1016/j.jneumeth.2008.08.011

A New Method of Spike Modelling and Interval Analysis

D. J. MacGregor, C.K.I. Williams* and G. Leng

Centre for Integrative Physiology, University of Edinburgh, Edinburgh EH8 9XD, UK, * Institute for Adaptive and Neural Computation, University of Edinburgh, Edinburgh EH1 2QL, UK.

Correspondence should be addressed to:

Professor Gareth Leng
Centre for Integrative Physiology
University of Edinburgh
Hugh Robson Building
George Square
Edinburgh EH8 9XD, UK

email: gareth.leng@ed.ac.uk
telephone: +44(0)131 650 2869

Key words: spike interval, histogram, modelling, spike train, log likelihood, oxytocin

Full Length Report

19 pages, 12 figures and 5 tables

Richard Dyball, University of Cambridge, red1000@cus.cam.ac.uk

Department of Physiology,
Development and Neuroscience
University of Cambridge
Downing Street
Cambridge
UK

Tel: +44 (0)1223 333756
Fax: +44 (0)1223 333786

Jianfeng Feng, University of Warwick, Jianfeng.Feng@warwick.ac.uk

Centre for Scientific Computing
University of Warwick
Coventry CV4 7AL
UK

Tel +44 (24) 765 73788
Fax +44 (24) 765 73024

William E. Armstrong, University of Tennessee, warmstrong@utmem.edu

The University of Tennessee Health Science Center
855 Monroe Avenue, Suite 515
Memphis, TN 38163
US

Tel +1 (901) 448-5995
Fax +1 (901) 448-7193

Colin Ingram, University of Newcastle-upon-Tyne, c.d.ingram@ncl.ac.uk

School of Neurology, Neurobiology and Psychiatry,
University of Newcastle upon Tyne
Medical School
Framlington Place
Newcastle upon Tyne NE2 4HH
UK

Tel +44 (0) 191 222 8210

Introduction

In general, neurons code information as patterns of spike activity. These patterns in part reflect patterning in the current input activity, but they also reflect intrinsic membrane properties of the neuron, and perhaps most importantly, spike activity itself can alter these properties, and how a neuron will respond to its inputs. Such changes occur over different time scales and via different mechanisms in different neuronal types, and as a result, different neuronal types have different capacities for processing information. Accordingly, understanding how information is coded in a particular neural network requires understanding the information processing abilities of each neuronal type from which the network is constructed. Here we seek to show how a concise computational model of the information processing capacity of a single neuronal type can be constructed from recordings of trains of action potentials.

In particular, oxytocin neurons in the rat discharge under the influence of randomly arriving excitatory and inhibitory postsynaptic potentials (EPSPs and IPSPs) (Armstrong, 1995). When EPSPs summate to trigger a spike, the resulting calcium entry into the cell triggers the opening of calcium-activated potassium channels, resulting in a hyperpolarising after potential (HAP) that makes the cell relatively inexcitable for typically about 50 ms after a spike. This is a relative, time-dependent inexcitability, and we have previously shown that its effects can be mimicked in a modified leaky integrate and fire model of a neuron by assuming that a spike instantaneously raises the spike threshold, and that this change decays exponentially.

However, the HAP is not the only activity-dependent conductance change that affects cell excitability. When strongly activated to fire repeated spikes, the membrane potential of oxytocin cells shows a deep, prolonged hyperpolarisation called the afterhyperpolarisation (AHP). This hyperpolarisation, it is thought, is the result of the temporal summation of small, prolonged hyperpolarisations that accompany each spike (Stern and Armstrong 1996).

Thus oxytocin cells are thought to have at least two distinct mechanisms that produce post-spike hyperpolarisations, with different dynamical characteristics. Here, we asked whether it is possible to detect the separate influences of the two similar mechanisms simply by analysing the spontaneous discharge characteristics of oxytocin cells. We show that oxytocin cells have spontaneous discharge characteristics that can be well fit by a leaky integrate-and-fire model that incorporates both an HAP and an AHP, but which cannot be fit by models with a HAP alone. We show how a simplex search algorithm can be applied to spike train data to estimate the best fit to parameters for the HAP and AHP, and show the limits of effectiveness of the algorithm by testing it

on data generated by a model. The methods that we show here are generalisable to analysis of any neuron whose recorded activity is governed by random inputs subject to deterministic activity-dependent effects on excitability.

Materials and Methods

The oxytocin cell model is a modified "leaky integrate-and-fire model" (Tuckwell, 1988); it simulates the firing response to Poisson randomly timed, exponentially decaying, input pulses, representing excitatory and inhibitory post-synaptic potentials (EPSPs and IPSPs) at mean rates I_{re} and I_{ri}; the IPSP frequency I_{ri} can be defined as a proportion of I_{re} given by I_{ratio}. Two variables, v and Θ represent the membrane potential and the spike threshold. t_s gives time since the last spike. EPSPs and IPSPs in oxytocin cells have a magnitude of 2-5 mV and last for 5-10 ms, and here we assume that at resting potential EPSPs and IPSPs have equal and opposite magnitude (4 mV) and a half life of 7.5 ms. Reversal potentials for EPSPs and IPSPs, v_e and v_i, are set at –38mV and –72mV from estimates in (Randle et al., 1986). Their amplitudes e_h and i_h are defined:

$$e_h = a(v_e - v) \tag{1}$$

$$i_h = b(v_i - v) \tag{2}$$

where a = 0.4 and b = 0.04. The Poisson random process generates PSP counts e_n and i_n at each time step to give summed input:

$$I = e_h e_n + i_h i_n \tag{3}$$

The resting potential, v_{rest}, and spike threshold at rest, Θ_0, for oxytocin cells are – 62 mV and – 50 mV (Bourque and Renaud, 1990). Membrane potential v is defined :

$$\frac{dv}{dt} = I - \gamma(v - v_{rest}) \tag{4}$$

where γ is the PSP half life (7.5ms), equivalent to leak conductance.

When v exceeds the spike threshold, Θ, the neuron fires a spike and the spike interval is recorded. A refractory period, caused by the HAP, is simulated by increasing Θ and allowing this to decay exponentially. k_H and λ_H define the HAP magnitude and decay rate to give

$$\Theta = \Theta_0 + k_H e^{-\lambda_H t_s} . \tag{5}$$

An extended version of the model adds an AHP, modelled like the HAP, but with the residual at the end of each ISI summed with the AHP generated by the next spike. Formally, the AHP at time t is defined as the sum of all previous AHPs, $\sum_i k_A e^{-\lambda_A(t-t_i)}$ where k_A and λ_A define the magnitude and decay rate and t_i is the time of spike i. Its implementation uses the equivalent recursive form where the AHP following spike i is defined $(k_A + AHP_{i-1})e^{-\lambda_A t_s}$ with AHP_{i-1} as the residual. This gives

$$\Theta = \Theta_0 + k_H e^{-\lambda_H t_s} + (k_A + AHP_{i-1})e^{-\lambda_A t_s} . \quad (6)$$

The default parameters for the HAP ($k_H = 60$, $\lambda_H = 0.1$), I_{re} (300Hz) and I_{ratio} (1), produce a firing rate in the normal range for oxytocin cells. These values were previously used to fit the model with just the HAP to real spike data, by matching firing rate and ISI distributions (Leng et al., 2001). The model uses a 0.1ms step size and was implemented in Visual C++ (Microsoft Corp., US). Simulations were run for 1000-100000s of simulated activity.

1.1. Experimental Data

The spike data used for comparison with the model consists of five recordings from different sources, but all in-vivo extracellular recording of basal activity in oxytocin cells of anaesthetised rats. They vary from 5000 to 100000 spikes. Most of the results presented use a single recording as an example, but all recordings showed similar features and results.

1.2. Spike train analysis

We examined the relationship between the timing of a spike and the activity immediately before. We looked at all ISIs of a particular length (T0) and compared them with the mean previous ISI (T1). The analysis was extended by examining trains of ISIs, plotting the mean sum of their lengths against T0 to test whether the effect might accumulate. To generate a fit measure, we calculate the probability of each individual ISI length based on the preceding ISIs. A reduced version of the model takes a series of ISIs and simulates the AHP following each spike to produce a final AHP value. This AHP value is then used to run the model for a single spike firing. By repeatedly running the model, a histogram is generated showing the probability distribution of ISIs following the train of ISIs from the real data. This histogram is then used to get an approximate probability for the actual ISI length. This is repeated for each ISI in the real data, and the log probabilities of each ISI are summed to give the log likelihood:

$$\log L(\mathrm{X}) = \sum_i \log(P(\delta_i \mid \delta_{i-20}, ..., \delta_{i-1}, \mathrm{X})) \quad (7)$$

where X is the set of parameters and $\delta_{i-20},\ldots,\delta_{i-1}$ are the 20 most recent ISIs, enough to estimate the current AHP. The log likelihood gives a measure of how well a particular set of parameters fits the data, taking into account dependence of spike response on previous firing activity.

The histograms are usually generated from 10000 spikes and use 10ms bins. A smaller bin width gives a more exact match to the ISI length being tested but increases error due to the limited number of spikes. Varied bin widths are tested in Fig. 4 showing little variation in the log likelihoods. Binning the histogram on a non-linear scale was also tested (not shown) but made no difference to results. In addition, rather than generating a histogram for each spike in the recorded data, approximately 100 histograms are generated covering the range of detected AHP values. Detected AHP values are binned with width varying from 0.01mV to 0.5mV depending on their range, though AHP parameters in a normal physiological range will use a bin no larger than 0.05mV. These approximations increase error in the log likelihood but are necessary to reduce computation time.

1.3. Simplex search

This is a standard multiple parameter search algorithm called the *downhill simplex method* (Nelder and Mead, 1965). In this algorithm, an initial set of parameter vectors forms an apex of points (in the search space, with each varied parameter a dimension) that vary from the apex in just one dimension. The simplex moves through the search space, changing one point (parameter vector) at a time, using several methods including stretching one point away from the others, reflecting itself, shrinking, or tilting onto another side. Its goal is to have all parameter vectors within a proportional range (defined by parameter *ftol*) of the best fit score. Initial parameter vectors are set up to cover the range of plausible parameter values. Its implementation is based on Press et al. (1992).

Results

1.4. Spike recordings and ISI histograms

The model with just the HAP was used to generate trains of 500000 spikes with varied parameters, to produce 1ms bin ISI histograms. Decaying exponential curves produced good fits ($P < 0.0001$) to the tail of each histogram using the equation $y = ae^{-bx}$, where x and y correspond to the

time and count axes of the histogram respectively.

Leng et al. (2001) recorded from oxytocin cells with different input activity controlled by varying hypertonic saline infusions. After fitting the HAP parameters by comparing ISI histograms with fixed input activity, the model was fitted to varied input activity data by varying I_{re}, with I_{ratio} fixed at 1; accordingly, our first tests varied I_{re}. At higher values of I_{re}, the firing rate is increased and the mode of the histogram is higher and earlier (Fig. 1a; I_{re} 150/s; firing rate 2.6 spikes/s; mode 66 ms, 1343 spikes; exp a = 1588, b = 0.0029; I_{re}, 500/s, 11.9 spikes/s; mode 44 ms, 6310 spikes; exp a, 17703, b = 0.0192). Varying I_{ratio} gives a similar result (Fig. 1b); increasing the IPSP rate has a similar effect as reducing the EPSP rate (I_{ratio} 0, 26.7 spikes/s; mode 29ms, 19511 spikes; exp a = 148363, b = 0.0649; I_{ratio} 1.5; 3.8 spikes/s; mode 67ms, 1919 spikes; exp a = 2507, b = 0.0043). To test whether increasing I_{re} can compensate for increased I_{ratio}, ISIs were generated with varied I_{ratio} and I_{re} adjusted to maintain a firing rate of 10 spikes/s. The distributions (Fig. 1c) are almost indistinguishable (I_{ratio}, 0, I_{re} 150/s, mode 49ms, 5537 spikes; exp a = 11873, b = 0.015; I_{ratio} = 1.5, I_{re} 870/s, mode 46ms, 5350 spikes; exp a = 11502, b = 0.014). A similar test varied v_{rest} and used I_{re} to compensate the firing rate (Fig.1d). Varying EPSP and IPSP amplitude or duration (not shown) also shows the same result. Thus it is clear that the firing rate dominates the form of the ISI histogram, and that differences in the structure of the input cannot be distinguished.

By contrast, differences in the HAP had readily distinguishable effects on the ISI distribution. The HAP is defined by its initial magnitude, k_H, and its decay rate, λ_H. With k_H at 60mV, λ_H was varied from 0.001 to 0.5 (half-life 693 to 1.4ms). A larger λ_H corresponds to a shorter HAP and higher firing rate (Fig.2a), and shifts the histogram mode to the left (Fig.2b) with a higher peak (λ_H = 0.01, 2.4 spikes/s, mode 351ms, 1862 spikes; λ_H = 0.5, 9.1 spikes/s; mode 11ms, 4935 spikes). As these are largely due to the change in firing rate, ISI histograms were generated with I_{re} adjusted to match a common firing rate of 7 spikes/s. The histograms (Fig.2c) still showed an earlier, smaller mode for a shorter HAP (λ_H = 0.07, mode 65ms, 3787 spikes; λ_H = 0.2, mode 32ms, 3524 spikes).

1.5. ISI Histogram Based Model Fitting

Previously, the model was fitted to data by varying I_{re} and λ_H, using I_{re} to match the firing rate and then adjusting λ_H to match the refractory period, by histogram matching (Fig 4a; fit λ_H = 0.11, I_{re} = 250). On the basis of the ISI histogram, matching input activity and the HAP is sufficient to fit the model, and reproduce cell firing behaviour. The histograms however don't preserve any information on spike ordering.

To detect any potential dependence on previous activity we developed a new analysis technique. If firing is independent, the current ISI T1 should show no correlation with the previous ISI, T0. We tested this on oxytocin cell recordings (Fig.5a); we found a negative correlation between mean T0 and T1 (fitted slope –0.074, $P<0.0001$). The effect is small, and large numbers of ISIs (about 1h of recording) are needed to detect it. The same analysis applied to fitted model generated data found no correlation (Fig 5c). The slope varies with longer trains of ISIs (Fig.5b); after an initial increase in the negative gradient for trains of up to 7 ISIs (from -0.07 to -0.26), the slope then reduces as the train becomes too long for earlier spikes to have an influence.

The AHP was added to the model in order to test whether it was sufficient to explain this effect.

1.6. The AHP augmented model

The AHP is much smaller than the HAP (~ 0.5mV after a single spike), and at physiological firing rates it might not be expected to have much effect. However, with $k_A = 0.5$ and $\lambda_A = 0.002$ (half-life 347ms) the model cell fires at 5.3 spikes/s vs 7.3 spikes/s without the AHP. Increasing k_A (Fig. 3a) reduces the firing rate, attenuates the histogram mode, and increases the number of longer ISIs ($k_A = 0$, 7.3 spikes/s; mode 50ms, 3763 spikes; $k_A = 1$, 4.3 spikes/s; mode 66ms, 1952 spikes). There is also a mode shift to the right, and an accompanying increase in gradient approaching the mode. Reducing λ_A (Fig. 3d) has a similar effect, though a smaller shift in the mode, ($\lambda_A = 0.0005$, 3.1 spikes/s; mode 56ms, 1466 spikes; $\lambda_A = 0.01$, 6.8spikes/s; mode 50ms, 3376 spikes). Removing the AHP's ability to accumulate across spikes produced a much smaller drop in firing rate (6.7 spikes/s at $k_A = 0.5$, 5.3 with AHP, 7.3 with no AHP). The ISI histograms (Fig.3c) show less change in the mode and similar numbers of long ISIs.

Adjusting I_{re} to match a firing rate of 7 spikes/s shows that k_A has little effect on the histograms (Fig. 3b), except for a slight attenuation of the mode as k_A increases. Thus, unlike the HAP, the AHP's effect on the ISI distribution is almost entirely due to its effect on firing rate. Results with varied λ_A are similar (Figs. 3e, 3f), there is no detectable effect of λ_A on frequency compensated ISI histograms, or with no AHP accumulation.

The effect of the AHP on firing rate indicated that the augmented model would have to be refitted. We started with the fit without the AHP ($\lambda_H = 0.11$, $I_{re} = 250$); adding the AHP and adjusting I_{re} to match the firing rate left a deficit of short ISIs, but reducing k_A and readjusting I_{re} produced a good fit (fit $\lambda_H = 0.11$, $I_{re} = 290$, $k_A = 0.3$, $\lambda_A = 0.002$). Importantly, a good fit did not require changing the HAP parameters (Fig.4b). The refitted model was then used to generate 5000

ISIs (Fig. 5d), and these showed a negative correlation between T1 and T0 (fitted gradient –0.079, $P<0.0001$, real data –0.074). Longer trains showed a similar initial increase in negative correlation (Fig. 6a), but not the reduction in correlation observed with real data (Fig. 5b) with very long trains, where repeated runs showed high variability and large error in the fitted gradients. Using more ISIs reduced the error (Fig. 6b, 100000 ISIs) but this much data is seldom available in experiments. The gradient effect at longer trains in the experimental data is consistent despite error, suggesting some effect not present in the model.

Thus the current technique cannot accurately detect the gradients of long ISI trains, but gives consistent results for shorter trains (~8 ISIs), and for these the AHP model matches the effect observed in real data. The main variation between experimental and model data is in the gradients fitted to longer trains. After the initial increase in negative correlation, experimental data show a reduction in negative gradients, which continues into positive values for trains of more than ~40 ISIs (not shown). It would be expected that with longer trains, including spikes beyond the range of the AHP's effect, the gradients should become less negative. There is some evidence of this in the model data (using very long spike trains, not shown) but less than in the experimental data. This was tested by using trains that start 10 ISIs before T0, (i.e. omitting spikes that correlate most strongly with T0). This should show no correlation (Fig. 6c) but in experimental data the positive correlation remained (Fig. 6d). This effect varies in magnitude between recordings, and probably indicates lack of stationarity in cell activity during the recording.

The main conclusion here is that the AHP is required to reproduce the patterning detected in experimental data but that its effect cannot be detected in ISI histograms, beyond variation in firing rate. A new fitting technique was required which takes account of previous spike activity.

1.7. Measuring fit over spike trains

For proof of concept of the 'log likelihood method', the model was used to both generate and fit the data. λ_A, k_A and I_{re} were varied individually to test the fit. In all cases, the best fit was at the known 'true' value, and the plots by their gradients (Fig. 7) indicate how difficult it might be to infer the true value from real data. λ_A shows a shallow gradient for values larger than the true value, indicating a range where it might be difficult to distinguish fits with different λ_A. The range of parameter values can be visualised by treating each parameter as a spatial dimension and plotting as points the fit measures for each set of values. Understanding this 'search space' can show how best to find the true values.

Fits were measured varying both k_A and λ_A. The contour plot (Fig.8) has a straight ridge,

indicating a linear relation between them (Fig. 9a). A larger k_A with a larger λ_A produces a similar fit to the data. This relation is called here $\rho_1 = k_A/\lambda_A$; $k_A = 0.5$ and $\lambda_A = 0.002$ give $\rho_1 = 250$. Analysis of the model predicts this relation; consider the AHP potential $a(t) = \sum_i k_A e^{-\lambda_A (t-t_i)}$ where the sum over i runs over spikes at times before t. If the t_i's are distributed according to a random process with mean rate μ, then the mean of $a(t)$ is $\bar{a} = \mu k_A \int_0^\infty e^{-\lambda_A t} dt = \mu k_A / \lambda_A$ (Cox and Miller, 1965). There is also temporal variability in $a(t)$, but if the main effect of the AHP is to build up to a roughly constant level $\bar{a} = \mu k_A / \lambda_A$ then ρ_1 is well-determined. The ridge has a peak at the true values (Fig. 9b), but error in the fit measure and the shallow gradient makes it difficult to find the exact maximum. Error in the fit measure depends on the ISI distribution, which in turn depends on the parameters. With $\lambda_A = 0.002$ and 50000 spikes over 100 runs, the mean log likelihood was –30499 with S.D. 4.73 (range –30486 to –30510), with a roughly normal distribution. With 10000 spike histograms, the mean was –30471 with S.D. 7.28 (range –30454 to –30488). The varied number of spikes also produces a small shift in the likelihood values, similar to the shift observed with varied histogram bin width (Fig. 7).

Fig. 10 shows the fit measures with varied k_A and I_{re}. Larger AHPs can be compensated by a higher I_{re}. Although there is no linear relation overall, there is a good linear fit near the best fit values (Fig. 11a); (P<0.0001) in the range $k_A = 0$ to 1. The best fit scores for each k_A, are maximal around the true value of 0.5 (Fig. 11b), and it would be possible to use this linear relation to make the parameter search more efficient. The linear fit gives the formula for the best fit $I_{re} = 225 + 150k_A$ where $I_{re} = 300$, $k_A = 0.5$ and $\lambda_A = 0.002$. Relating this to ρ_1 gives $\rho_2 = (I_{re}–225)/\rho_1 = 0.3$. More generally,

$$\rho_1 = k_A / \lambda_A \tag{8}$$

$$I_{re} = offset + \rho_1 \rho_2 \tag{9}$$

where the *offset* value in this case is 225.

The log likelihood gives a reliable fit measure that can detect and quantify the AHP's effect on spike patterning, although there is some error due to estimating the ISI probability distributions with model generated histograms. The two ratios ρ_1 and ρ_2 show the relation between AHP parameters and the input rate, and indicate the form of the parameter space.

1.8. Simplex Search

We used the *downhill simplex method* (Nelder and Mead, 1965) with the log likelihood fit measure (using 10000 spike histograms) to search the parameter space.

First attempts to retrieve true values ($k_A = 0.5$, $\lambda_A = 0.002$, $\rho_1 = 250$) from model-generated data initially varied just one parameter (Fig. 7). Parameter *ftol* was set at 0.0002. With fit scores for plausible parameter values in the range -28000 to -31000, the scores for the final set of points must be within ~ 6 units. To give the search algorithm a more linear range for λ_A, it uses the natural log value. Varying k_A and λ_A in turn found the true values (λ_A initial values 0.0009 and 0.497, final estimates 0.0019 and 0.0020; k_A initial values 0 and 5, final estimates 0.47 and 0.51).

Testing two parameter search, we varied k_A and λ_A, with three different sets (A, B and C) of initial parameter vectors (Table 1). Repeated runs showed some variation, so we tested 10 runs with each initial vector set, producing 30 estimate vectors for each initial set. Many estimates were duplicated; the results for set A consisted of only 13 unique estimate vectors. Results with likelihood less than the mean likelihood minus one standard deviation (approx 15% of the results) were rejected. For set A the mean estimate for k_A was 0.587 (range 0.398-0.887), for λ_A was 0.0023 (0.0017-0.0037) and for ρ_1 was 253 (205-281), with mean likelihood -30469. For set B the mean estimate for k_A was 0.731 (0.474-1.126), for λ_A was 0.0029 (0.0019-0.0037) and for ρ_1 was 256 (222-283), with mean likelihood -30472. For set C the mean estimate for k_A was 0.706 (0.420-0.982), for λ_A was 0.0027 (0.0017-0.0037) and for ρ_1 was 264 (214-298), with mean likelihood -30471. Table 1 shows the initial parameter vectors and the mean estimate vector for each initial set (A, B and C).

Estimate A is closest to the true values. Estimates B and C vary more, but have a ρ_1 close to the true 250, indicating that they fall on the k_A-λ_A ridge. Estimate A has the best score, though the error in the log likelihood score is too great to distinguish between results.

Testing three parameter search, we varied k_A, λ_A and I_{re}, with 10 runs of each of three different initial vector sets (A, B and C). The final estimates, because parameters are not independent, can not use the mean estimate for each parameter. They use the mean estimates for ρ_1 and I_{re} to calculate ρ_2 using (9). λ_A is calculated from (8) using the mean estimates for k_A and ρ_1. The difference from the means is small, and negligible when varying only two parameters, hence ignored above. Set A estimated k_A 0.70, (0.32-1.01), λ_A 0.0033 (0.0016-0.0069), ρ_1 214 (92-417), I_{re} 285 (250-353) and ρ_2 0.279 (0.216-0.365), mean likelihood -30480. Set B estimated k_A 0.63, (0.32-1.04), λ_A 0.0015 (0.0011-0.0022), ρ_1 409 (315-509), I_{re} 348 (307-386) and ρ_2 0.303 (0.259-0.339),

mean likelihood -30472. Set C estimated k_A 0.67, (0.54-0.76), λ_A 0.0016 (0.0014-0.0019), ρ_1 414 (341-492), I_{re} = 351 (322-385) and ρ_2 0.306 (0.282-0.338), mean likelihood -30471. B and C overestimate the size and duration of the AHP, and I_{re}. The larger I_{re} compensates against the larger AHP, thus the estimated ρ_1 is higher than the true 250, but the estimated ρ_2 is close to the true 0.3. Estimate A shows the opposite effect, a small AHP (ρ_1 less than 250) compensated by a lower I_{re}. Table 2 shows the initial parameter vectors and final estimates for each initial set (A, B and C) (ρ_2 is undefined when $k_A = 0$).

All three sets produced estimates close to the true values. Sets B and C get a closer match to ρ_2 and show better likelihood scores than Set A. Another test used a new dataset with $k_A = 0.3$ and $I_{re} = 350$, giving a true $\rho_1 = 150$. Plotting the true best fit values for I_{re} with varied k_A gives $\rho_2 = (I_{re} - 384) / \rho_1$, with true $\rho_2 = 0.44$. Parameter search was tested using 10000 ISI histograms, and three initial parameter sets (Table 3). All three results overestimate the AHP, with a corresponding large ρ_1, but ρ_2 is close to the true 0.44 in all tests, compensated by an increased I_{re}. Initial set B gives ρ_1 and ρ_2 closest to the true values, and has the best likelihood scores.

Finally three parameter search was tested on five more varied model generated sets of 10000 spikes, using 3 runs of 4 initial parameter sets, and 20000 spike histograms. The datasets' true parameters and final estimates are detailed in table 4, with full results plotted in Fig. 12, showing the consistent linear relation ρ_2 between I_{re} and ρ_1. In each case the range of estimates includes the true values though some tend to under or over-estimate the size of the AHP. This range corresponds to the peak in Fig. 11b where error in the log likelihood makes it difficult to distinguish a unique best fit. The final estimates use the mean estimate for ρ_1 and the values for the fitted line's gradient (ρ_2) and origin (*offset*) to calculate I_{re} using (9). λ_A is calculated from (8) using the mean estimates for k_A and ρ_1.

The average computing time for the current implementation on a single AMD Opteron 2.6Ghz processor for one run of the simplex search using 20000 spike histograms and three varied parameters is approximately 100 minutes, totalling 20 hours for the twelve runs on each dataset. Computing time varies mainly with the average firing frequency produced by a parameter set.

The simplex gives an effective and economic method for finding a good fit to ISI data. Results on repeated runs and with different initial vectors can vary, but can all be related by ratios ρ_1 and ρ_2.

1.9. Initial Tests with Experimental Data

These results are a first attempt to see how well fitting might work outside the well controlled model-generated data. The fit version of the model was run with default parameters, varying k_A, λ_A and I_{re}, using the ISI histograms to pre-fit the HAP. Log likelihood probability distribution histograms for simplex fitting were generated from 10000 spikes. Five sets of experimental data were each tested with three identical runs of four initial parameter sets, producing twelve estimates for each dataset. The estimates showed some variation, but for each dataset a plot of each estimate's ρ_1 against I_{re} could be fitted by a straight line (all $p < 0.0001$), indicating a consistent ρ_2, and that the experimental data maintains the relationships observed in model data. To get a final estimate for each dataset we took the mean of the best six according to fit scores; shown in Table 5. Generating model data using the simplex estimated parameters produced very close fits to the experimental data's ISI histograms, and closely matched firing rates, confirming the fits on these bases. Across the datasets, the fitting produced estimates for the AHP parameters, and input rate, within a consistent and physiological range.

Discussion

This work began with an augmented leaky integrate and fire model with added HAP, similar to the spike response model of Gerstner (1995), fitted to recorded spike intervals on the basis of comparing ISI histograms. This assumes that the timing of each spike is independent of previous activity. The new spike train analysis technique applied to recorded data shows a correlation between the length of current and previous intervals, indicating that this assumption is not valid.

The cell component suspected of producing this effect is the AHP. This is a small current, but its long time course allows it to accumulate and have a substantial effect on firing threshold. Adding the AHP to the model was able to reproduce the correlation. The effect of the AHP can be detected in the ISI histogram, but cannot be distinguished from other parameters which alter the firing rate, so a new fitting process was developed which retains information based on spike ordering, and is able to detect the AHP's effect on proceeding spike intervals.

We investigated how neuronal properties (as implemented in the model) influence the ISI distribution. Parameters that directly control the firing rate, (I_{re}, firing threshold and the ratio of IPSPs) have equivalent effects on the distribution, so only one of these needs to be adjusted for fitting. The more subtle aspects of the distribution, such as the gradient at the front end, relating

particularly to the HAP and AHP can be isolated by adjusting I_{re} to compensate for varied output rates. This was used for a fitting scheme where a matched firing rate is maintained by adjusting I_{re} to compensate for adjustments in the HAP or AHP parameters. The varying effect of the HAP can be observed in the front of the histogram, with slower decay (λ_H) indicated by a mode shifted to the right, with fewer short ISIs. The model can be reliably fitted to real data to estimate the HAP decay.

The AHP, with its ability to accumulate, has a significant effect on the ISI histogram, reducing the firing rate and increasing the number of longer ISIs. However, unlike the HAP, it is very difficult to distinguish the effect of the AHP from changes in I_{re}. With the ISI histogram the model with the AHP can be fitted without altering the fitted HAP parameters, adjusting I_{re} to maintain firing rate. Though a good fit is produced, the AHP's parameters cannot be uniquely determined, since it cannot be distinguished from other effects on firing rate.

Spike train analysis provides a new method to analyse firing patterns which can detect a relationship between the firing times of adjacent spikes. Applying spike train analysis to spike timings from a recorded oxytocin cell detects a correlation such that a short ISI is more likely to be followed by a longer ISI and vice versa, indicating that the cell 'remembers' previous firing activity and regulates its own firing rate. Applying this analysis to the model with just the HAP finds no such correlation. Adding the AHP produces a similar effect to the real data, suggesting that the AHP is responsible in real cells. This also suggests that the AHP's effect can be measured by looking at intervals in the context of previous spike activity.

The final work begins the development of a more sophisticated fitting technique which takes account of the relation between adjacent spike timings. The log likelihood measure produces a measure of fit between a reduced version of the model (modelling a single spike interval based on recorded previous intervals) and a real cell recording. Simplex search is then used to gradually adjust multiple model parameters to find the best fit to the real data. This is however very computationally expensive. Work has focused on attempting to understand how the model parameters relate to how well the data is fitted to develop a more heuristic based approach. A linear relationship between the two AHP parameters has been detected, making it possible to reduce these to a single ratio value (ρ_1) for a first stage of searching. Further to this, there is within a limited range a linear relation (ρ_2) between the ratio of the AHP parameters and the spike input rate, also of potential use to limit parameter search. These ratios can also be used to relate the varied parameter estimates produced by repeated runs of simplex search.

Contemporary theoretical work in Paninski et al. (2004), also uses the leaky integrate and fire model as a basis, along with a likelihood method for fitting the model. They make a similar

conclusion on the importance of post-spike potentials for reproducing the features of recorded firing patterns. Their model however retains a simplified form with a single term for the post-spike potential and a purely white noise based input signal in order that the likelihood measure can be computed without using simulation. This gives a more efficient fitting method but with the disadvantage that the input signal may be less well modelled. The input signal in our model is based on random pulses but its mix of excitatory and inhibitory decaying pulses gives some structure important to the linear relationship between input rate and firing rate. Purely excitatory input produces a much more non-linear relationship (Feng and Brown, 1999).

Early results here, using the simplex method to fit real data, produce reasonable values for the AHP and for the input rate. Running the model with these values also produces good fits to the ISI histograms. Further tests will need to vary more parameters to test how robust these estimates are. Methods also need to be developed to test these estimates in comparison with other analysis of the cell recordings. If the fitting process is sufficiently reliable, this will provide a powerful tool for the analysis of cell recordings, being able to infer intrinsic properties which are not otherwise accessible, particularly *in-vivo*, providing a non-invasive method for identifying cells.

Acknowledgements

This research was supported by grants by the European Union Framework Programme VI Integrated Project (LSH-CT2003-503041), and from the BBSRC.

References

Armstrong WE. Morphological and electrophysiological classification of hypothalamic supraoptic neurons. Prog Neurobiol 1995;47:291–339.

Bourque, C. W. and L. P. Renaud. Electrophysiology of mammalian magnocellular vasopressin and oxytocin neurosecretory neurons. Front Neuroendocrinol 1990;11(3):183-212.

Cox DR, Miller HD. The theory of stochastic processes. Methuen: London, 1965.

Feng J, Brown B. Coefficient of variation of interspike intervals greater than 0.5. How and when? Biol Cybern 1999;80:291–7.

Gerstner, W. Time structure of the activity in neural network models. Phys Rev. E. 1995;51:738-58.

Leng G, Brown, CH, Bull PM, Brown D, Scullion S, Currie J, Blackburn-Munro RE, Feng JF, Onaka T, Verbalis JG, Russell JA, Ludwig M. Responses of magnocellular neurons to osmotic stimulation involves coactivation of excitatory and inhibitory input: An experimental and theoretical analysis. J Neurosci 2001;21(17):6967-77.

Nelder JA, Mead R. A simplex method for function minimization. Computer Journal 1965;7(4): 308-13.

Paninski L, Pillow JW, Simoncelli EP. Maximum likelihood estimation of a stochastic integrate-and-fire neural encoding model. Neural Comput 2004;16:2533-61.

Press WH, Teukolsky SA, Vettering WT, Flannery BP. Numerical recipes in C, 2nd Ed. Cambridge University Press, 1992.

Tuckwell, H. C. Introduction to theoretical neurobiology. Vol 2, Cambridge University Press, 1988.

Randle JCR, Bourque CW, Renaud LP. Characterization of spontaneous and evoked inhibitory postsynaptic potentials in rat supraoptic neurosecretory neurons invitro. J Neurophysiol 1986;56(6):1703-17.

Stern JE, Armstrong WE. Changes in the electrical properties of supraoptic nucleus oxytocin and vasopressin neurons during lactation. J Neurosci 1996;16(16):4861-71.

Figure Legends

Figure 1. **ISI histograms with varied input spike parameters.**

Histograms generated from 50000 spikes.

a. Increased input frequency (I_{re}) increases the firing rate and shifts the histogram towards a higher proportion of short spike intervals, with a higher mode shifted to the left (I_{re} range 150 to 500Hz, highest mode = highest I_{re}).

b. An increased proportion of IPSPs (I_{ratio}) has the opposite effect, reducing firing rate and increasing the number of long spike intervals, with a lower mode shifted to the right (I_{ratio} range 0 to 1.5, highest mode = lowest I_{ratio}). Reducing I_{ratio} shows a similar effect to increasing I_{re}.

c. ISI histograms show no variation when I_{re} is varied to fix the output frequency (frequency compensation, here fixed at 10Hz) while varying I_{ratio} (range 0 to 1.5).

d. Similarly, varying v_{rest} to adjust cell sensitivity, with frequency compensation shows matching histograms.

Figure 2. **Output rate and ISI histograms with varied HAP decay rate**

a. An increased HAP decay rate, reducing HAP duration, has a large effect on firing rate, with a four-fold increase between λ_H= 0.001 and λ_H = 0.2 (figure shows λ_H range 0.01 to 0.5).

b. Overlaid ISI histograms with varied λ_H (range 0.01 to 0.5, highest mode = largest λ_H) show the mode increasingly shifted to the left, with the longer lasting HAP increasing the refractory period.

c. Overlaid ISI histograms varying λ_H with I_{re} adjusted to match output frequency (7Hz, highest mode = smallest λ_H). Removing the effect of firing rate still shows the mode shifted to the left with the longer duration HAP (smaller λ_H), showing the longer refractory period. With I_{re} increased to compensate, the HAP is overcome more quickly after the refractory period, with HAP affected intervals falling in a shorter period, with a higher mode. The tails of the histograms, where the interval is too long for the HAP's effect to remain, match, following a Poisson distribution.

Figure 3. ISI histograms with varied AHP parameters

a. Overlaid ISI histograms with varied AHP magnitude (k_A, range 0 to 1mV, highest mode = lowest k_A) show with increasing k_A fewer short intervals, reducing the height of the mode and slightly shifting it to the right, similar to the change observed with reduced I_{re} in figure 1a, suggesting dominance by firing rate.

b. This is confirmed by using frequency compensation to show no variation between histograms

with varied k_A and matched firing rates, though on close inspection lower k_A values do show a slightly higher mode.

c. With no AHP accumulation between spike intervals most of the effect of k_A is removed, with a lower k_A still showing a slightly higher mode. This demonstrates that the major effect of the AHP is based on its ability to accumulate rather than the AHP generated by individual spikes.

d. Similar to a. but varying the AHP decay rate (λ_A, range 0.0005 to 0.01, highest mode = highest λ_A), the longer duration AHP produces fewer short intervals, similar to reduced I_{re}.

e. Using frequency compensation to eliminate the effect of firing rate also matches the histograms with varied λ_A.

f. Again, taking away AHP accumulation between spikes almost eliminates its effect in the histogram, even more so with varied decay rate than initial magnitude (k_A).

Figure 4. **The model fitted to experimental data**

Experimental dataset mludw1 (5206 spikes recorded from an oxytocin cell, mean frequency 5.79Hz)

a. The basic model (no AHP) was fitted by eye by adjusting λ_H, and with each adjustment, re-matching the firing frequency of the recording by adjusting I_{re} ($I_{re} = 250$, $\lambda_H = 0.11$). On the basis of the ISI histogram the basic model without the AHP very closely fits the experimental data.

b. The model with the AHP was fitted using a similar process, beginning with the fit in **a**. The previously fitted HAP parameters did not have to be adjusted. The AHP was fitted by fixing λ_A and adjusting k_A and again adjusting I_{re} to maintain the output frequency. A very close fit to the histogram is obtained ($I_{re} = 290$, $\lambda_H = 0.11$, $k_A = 0.3$, $\lambda_A = 0.002$).

c. The normalised cumulative distributions corresponding to **a**. show a very close fit between recorded data and model. The maximum distance between distributions is 0.01480.

d. The normalised cumulative distributions corresponding to **b**. similarly show a very close fit between recorded data and model. The maximum distance between distributions is 0.01249.

Figure 5. **Spike train analysis and fitted gradients**

a. Here spike train analysis is applied to the recorded data fitted in fig 4. Binned spike interval lengths (T0) are plotted against the mean previous interval length (T1), and a line fitted using linear regression, showing a downward slope indicating a negative correlation between T0 and T1, thought to be caused by the AHP.

b. Plotting fitted gradients (shown with estimated fit error) for progressively longer spike trains (T1,

T1+T2, etc.), shows an initial steep increase in correlation followed by gradual decay back to no correlation. The fit is only statistically significant up to 13 intervals in the spike train. The effect of the AHP lasts over several spikes, so that a longer train of previous spikes initially increases the correlation until the train is long enough the include spikes whose AHP contribution has already decayed.

c. The same analysis as in a. applied to the fitted model data from fig 4 (modgen3, no AHP) shows no correlation. This also demonstrates that fitting based on the ISI histogram is not sufficient to account of effects such as the AHP.

d. The AHP was added to the model and refitted to the experimental data (model $\lambda_H = 0.11$, $I_{re} = 290$, $k_A = 0.3$, $\lambda_A = 0.002$). Spike train analysis now shows a significant negative correlation between T0 and T1, supporting the hypothesis that the AHP is responsible.

Figure 6. **Effect of error and variation between model and recorded data**

a. Five identical runs of the fitted model generating 5000 spikes show a large variation in fitted gradients, particularly for longer spike trains. The plots show similar initial steeper gradients indicating increasing negative correlation with longer spike trains to the recorded data in fig 5b but do not show a consistent recovery in gradient with very long spike trains.

b. Similar data, using 100000 spike runs of the model shows a much smaller variation between runs. Again, the model data shows steeper negative gradients over longer spike trains, but not the eventual increase in gradient observed in cell data at very long spike trains. Using even longer spike trains does show an eventual increase in gradient, but at a much slower rate than the cell data (not shown). Some gradient recovery (reduction in negative correlation) would be expected as the spike train includes more intervals which are too long previous to affect T0.

c. Here we use similar analysis but using spike trains starting at T10 (10 intervals before the current spike interval) intended to remove intervals which are recent enough to affect T0. With intervals too far previous to influence the AHP there is no correlation and the gradient is consistently close to 0.

d. Similar analysis to c. applied to recorded data. Removing the effect of the AHP removes the negative gradients at shorter spike trains, but continues to show increasing positive gradients. This explains the more rapid recovery towards a 0 gradient observed in recorded data spike trains starting at T1. Some other process present in the cell recordings must be responsible for the positive correlation, possibly variation in input rate over the recording.

Figure 7. **Log likelihood fit measure with varied model parameters and histogram bin width**

Here a model generated dataset ($I_{re} = 300$, $k_A = 0.5$, $\lambda_A = 0.002$) was fitted against the model

varying a single parameter. The true values used to generate the data are indicated by the dotted lines. Likelihood values are shown using a range of histogram bin widths to approximate probabilities. Results are very similar, with a small shift in values, but all peaking at the true parameter value. The larger 10ms bin gives a larger difference in likelihood between the true and neighbouring values.

a. Varying parameter λ_A. The linear scale, which is not well suited to decay rates, makes it difficult to identify the best fit.

b. as in a. but with the x-axis plotted on log scale. The best fit measure is at $\lambda_A = 0.002$, matching the true value used to generate data. The log likelihood shows a rapid climb from lower values of λ_A but a more shallow gradient over values higher than the true. In terms of parameter search this makes it more difficult to distinguish between fits at higher values.

c. Varying parameter I_{re}, the best fit is again at $I_{re} = 300$, the true value. Similar to λ_A, higher values than the true are more difficult to distinguish on the basis of the log likelihood fit measure.

d. Testing the fit against parameter k_A again shows the best fit at true value $k_A = 0.5$. Here values lower than the true are more difficult to distinguish. This is consistent with b., indicating that a smaller AHP, either by reduced magnitude, or increased decay rate is more difficult to distinguish by fit measure.

Figure 8. **Contour plot of fit measure varying k_A and λ_A**

The fit measure is indicated by colour, red = best fit, the log likelihood fit scores were offset to give a bigger proportional range of values around the best fits. The model was fit against model data generated with parameters $k_A = 0.5$ and $\lambda_A = 0.002$, similar to fig 7. The contours show a diagonal ridge indicating the best fits, and passing through the true values. The ridge becomes wider as k_A or λ_A increases, and the low gradient along ridge makes finding exact maximum difficult. Local peaks on the ridge correspond to parameter resolution rather than the true form but the ridge does show a peak at the true values. The ridge itself shows its own gradient, more precisely explored in fig 9. The black circle indicates the true values and the black line shows the ratio ρ_1.

Figure 9. **Best fits with varied k_A and λ_A**

For a range of values of k_A, log likelihood fit was measured over a range of λ_A values to find the best fit for each k_A value.

a. A plot of λ_A values corresponding to best log likelihood scores over a range of k_A values, shows a distinct linear relationship between the two parameters, corresponding to the ridge observed in figure 8. The linear relation can described by ratio $\rho_1 = k_A/\lambda_A = 250$.

b. A plot of the corresponding best log likelihood scores over k_A, showing the gradient along the ridge, does show a maximum but error in log likelihood scores means this covers a range of k_A (and corresponding λ_A) values, though it does include the true values $k_A = 0.5$ and $\lambda_A = 0.002$.

Figure 10 : **Contour plot of fit measure varying I_{re} and k_A**

The fit measure is indicated by colour, red=best fit with log likelihood scores offset to give a bigger proportional range of values around the best fits. The model was fitted against model generated data with parameters $k_A = 0.5$, $\lambda_A = 0.002$, $I_{re} = 300$. The contours show a diagonal ridge indicating best fits and passing through the true values the ridge curves slightly with increased k_A but appears almost linear in area of best fit. Local peaks on the ridge correspond to parameter resolution rather than the true form. The black circle indicates the true values and the black line shows the ratio ρ_2.

Figure 11. Best fits with varied I_{re} and k_A

a. The plot of I_{re} values corresponding to best log likelihood scores over a range of k_A values shows a distinct linear relationship between the two parameters ($p<0.0001$), corresponding to the best fit area of the ridge observed in fig 10.

b. The plot of the corresponding best log likelihood scores over k_A, shows the gradient along the ridge. This does show a maximum but variability in log likelihoods means this covers a range of k_A (and corresponding I_{re}) values.

Figure 12. Simplex search with varied model generated data

For each of 5 datasets 3 parameter simplex search is run 3 times with 4 initial parameter vectors, to produce a total of 48 fits for each dataset (4 in the final simplex from each run). The plot uses all points with a log likelihood which falls within one standard deviation of the mean log likelihood generated with the true parameters, between 50% and 75% of the 48 fits. The range of fits follows the linear relation between I_{re} and ρ_1 and corresponds to the peak observed in Fig. 11b. The true parameters for each dataset are indicated by the white circle.

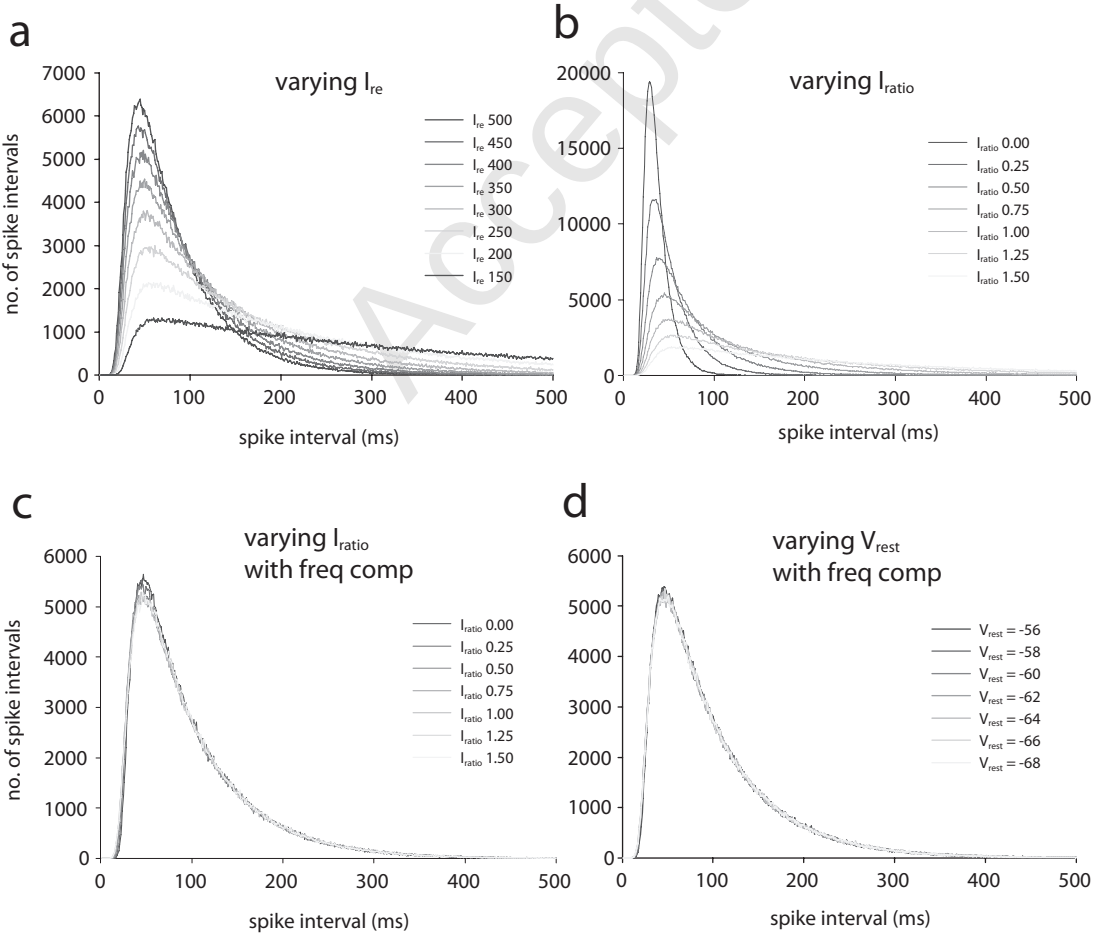

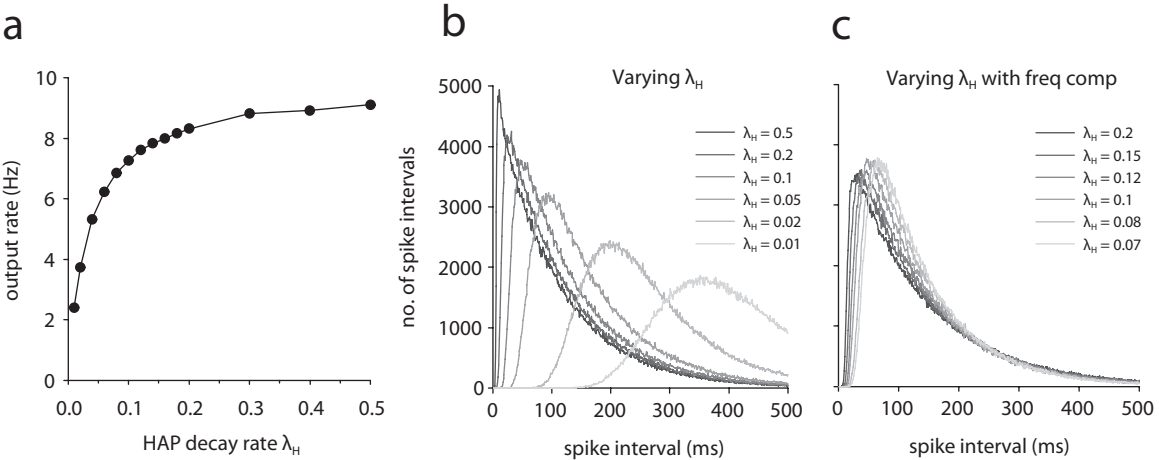

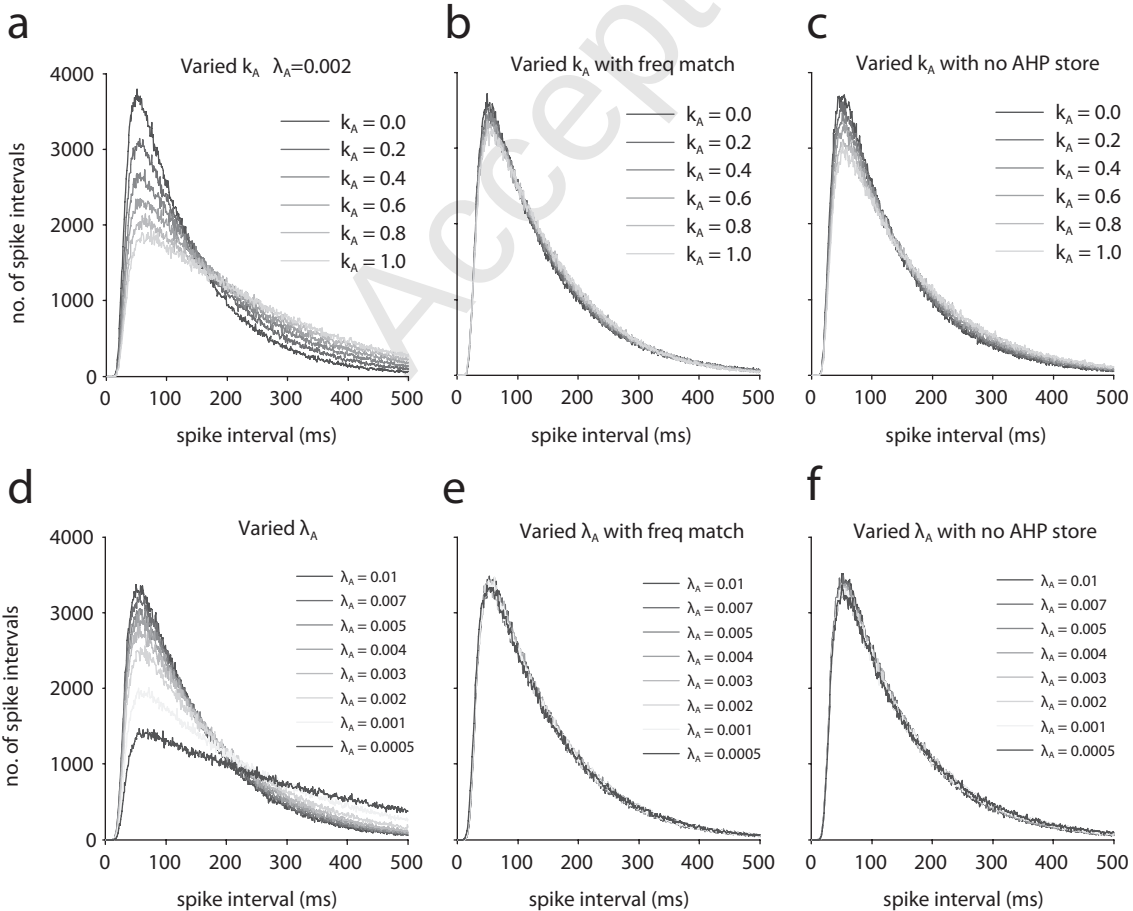

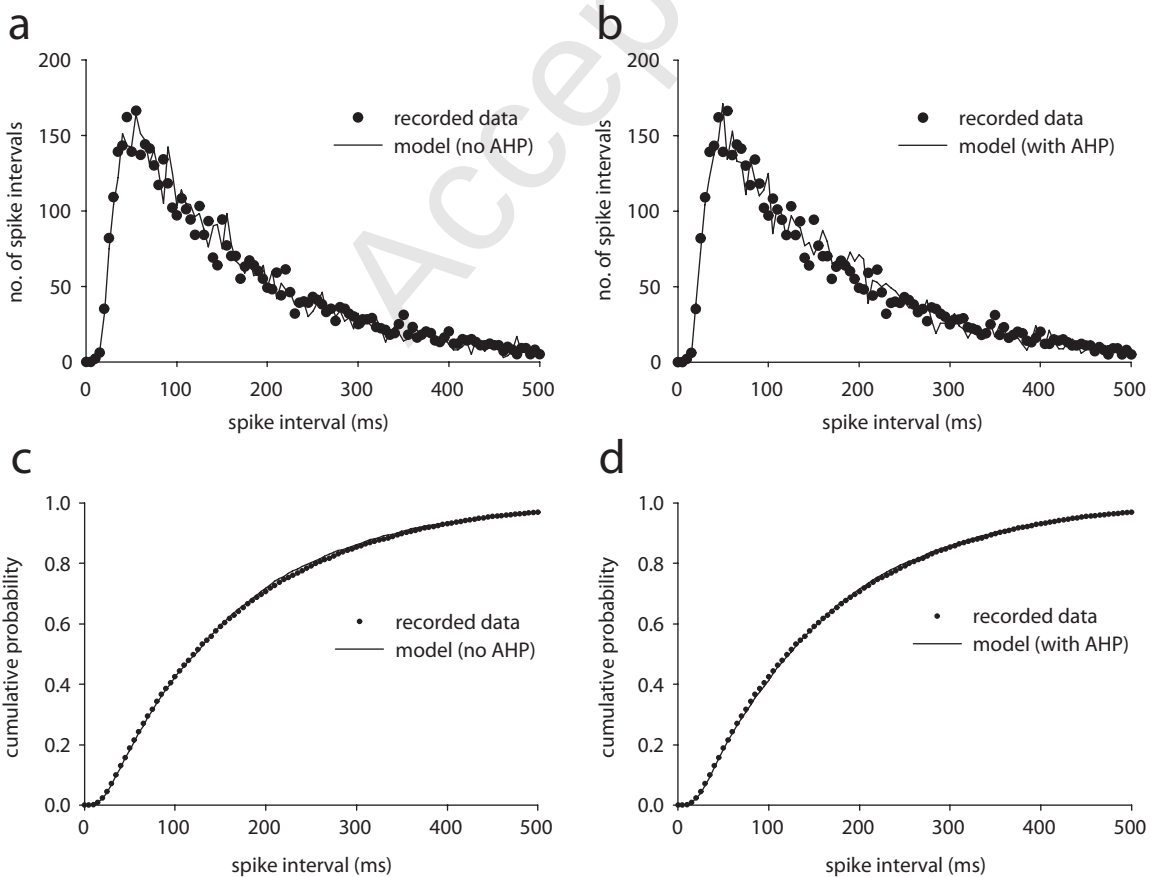

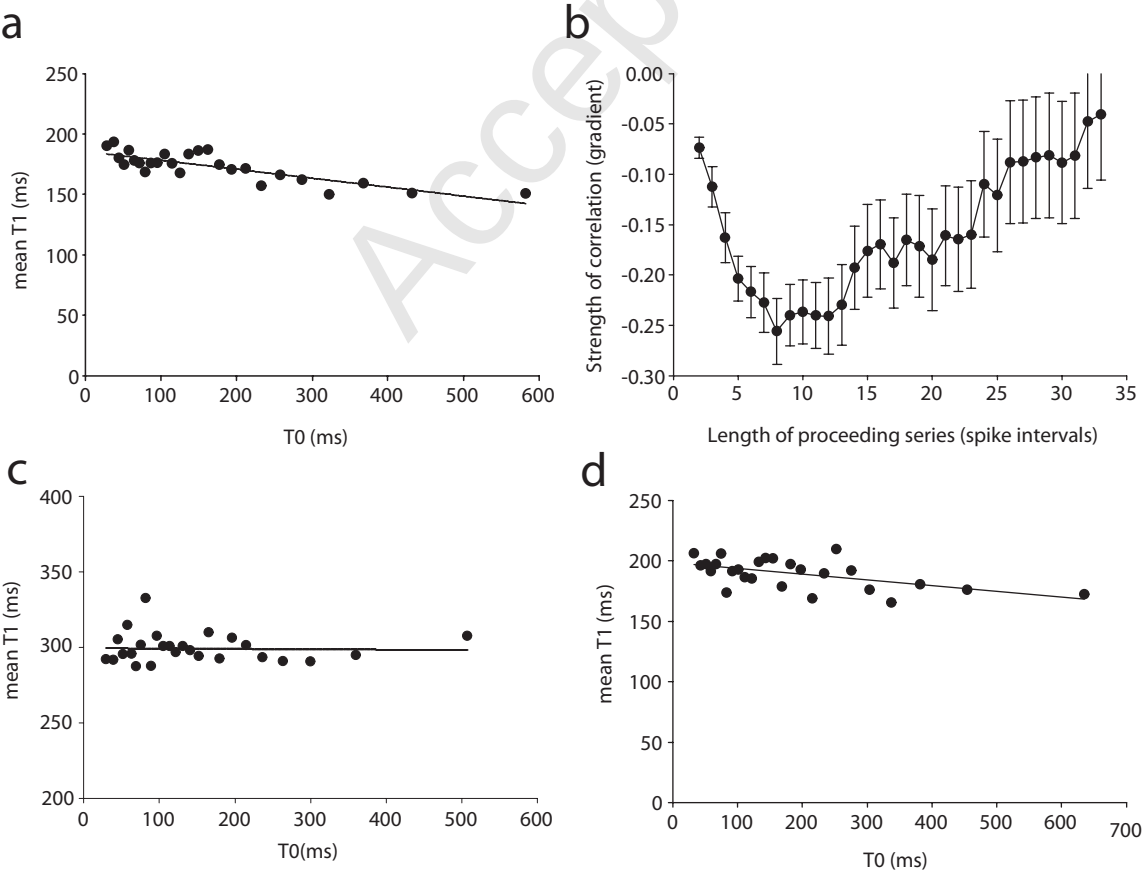

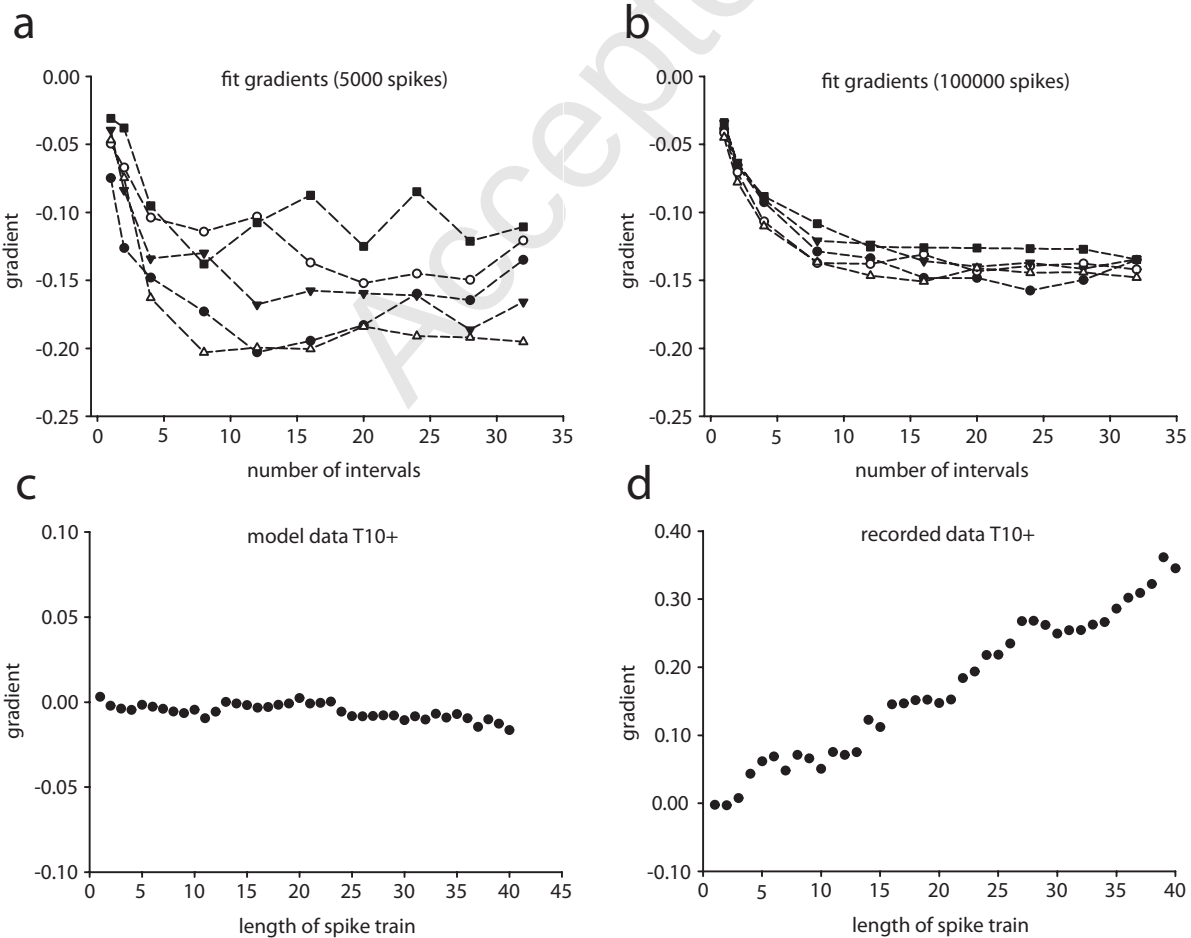

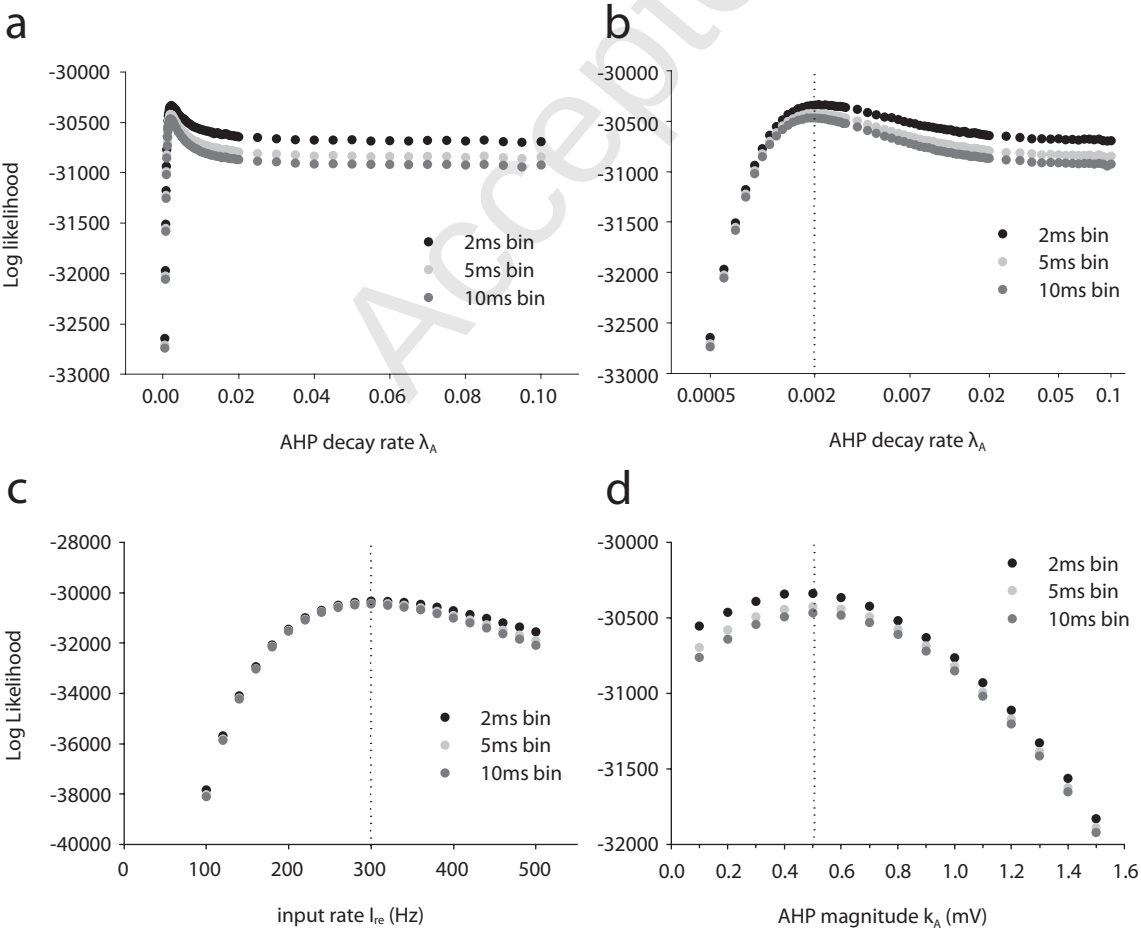

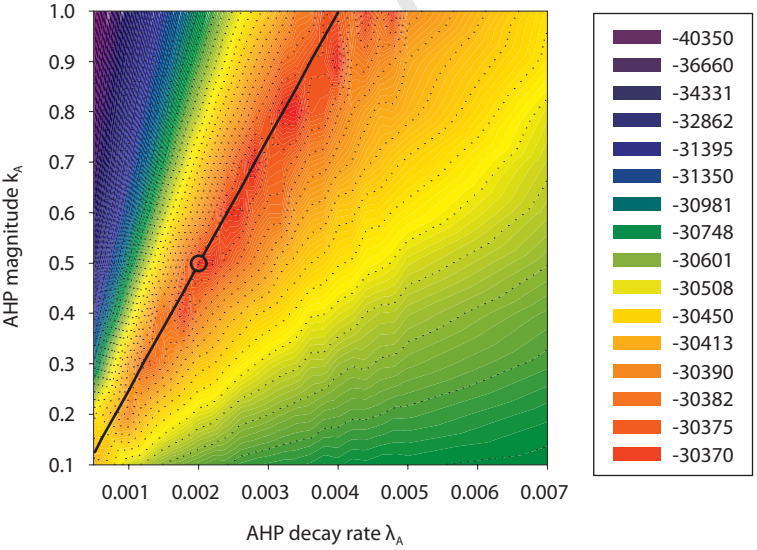

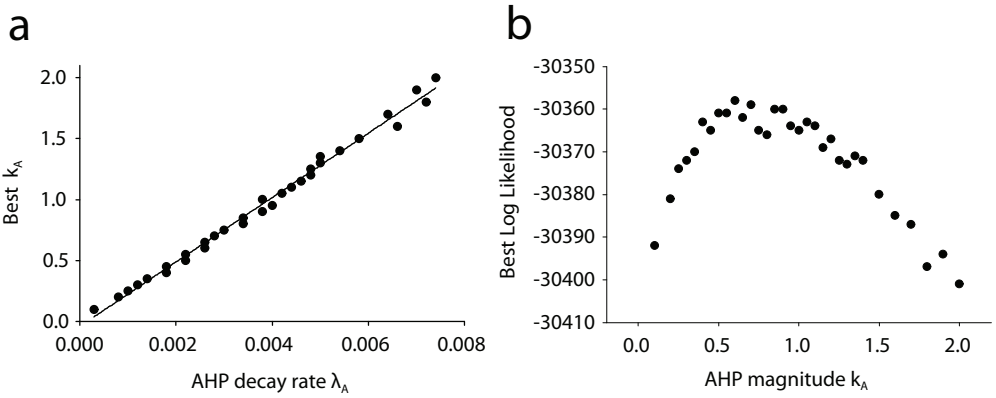

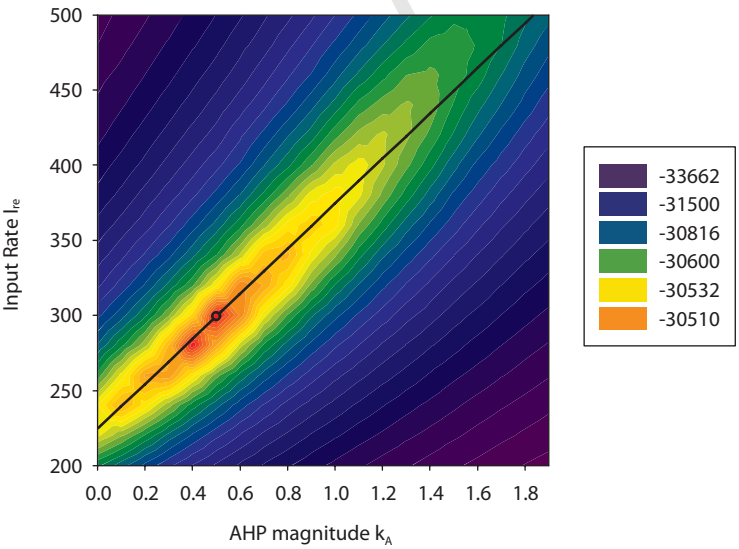

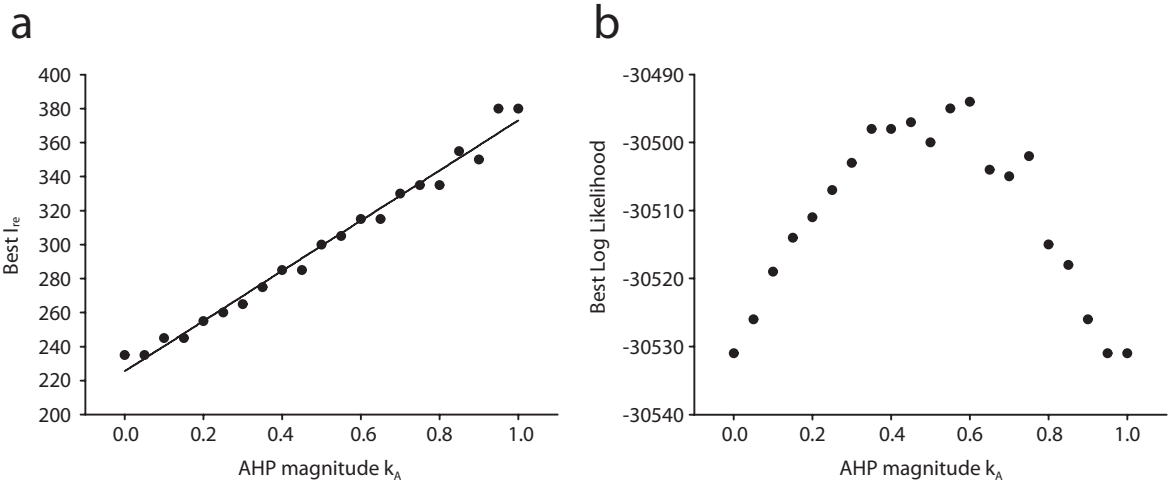

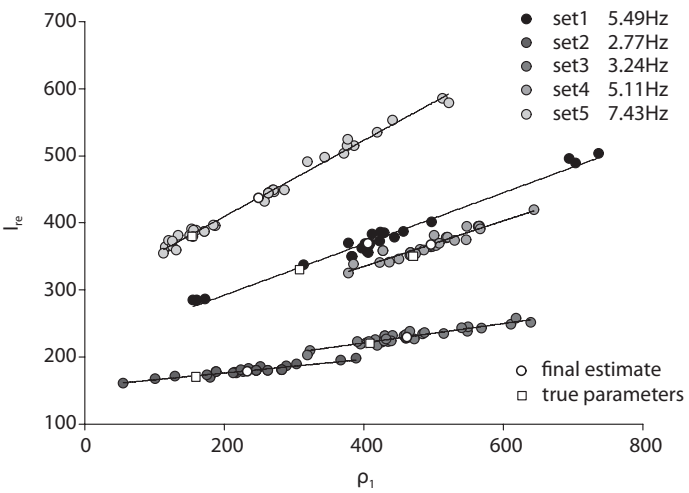

Table 1 : Simplex fitting estimates, varying λ_A and k_A

Vector	**λ_A**	**k_A**	**ρ_1**	**Log Likelihood**
Initial A1	0.00091	0.1	110	-30626
Initial A2	0.01111	0.1	9	-30907
Initial A3	0.00091	2.0	2198	-45208
Estimate A	0.00233	0.587	253	-30469
Initial B1	0.00091	0	0	-30932
Initial B2	0.01832	0	0	-30916
Initial B3	0.00091	5	5495	-57432
Estimate B	0.00286	0.731	256	-30472
Initial C1	0.00091	0	0	-30934
Initial C2	0.49659	0	0	-100000
Initial C3	0.00091	5	5495	-57430
Estimate C	0.00268	0.706	264	-30471
True	**0.00200**	**0.500**	**250**	**-30470**

Table 2 : Simplex fitting estimates, varying λ_A, k_A and I_{re}

Vector	λ_A	k_A	ρ_1	I_{re}	ρ_2	Log Likelihood
Initial A1	0.00091	0	0	100	-	-35247
Initial A2	0.01832	0	0	100	-	-35177
Initial A3	0.00091	5	5495	100	-0.023	-57565
Initial A4	0.00091	0	0	500	-	-33905
Estimate A	**0.00358**	**0.699**	**214**	**285**	**0.279**	**-30480**
Initial B1	0.00091	0.1	110	500	2.51	-33114
Initial B2	0.01832	0.1	5.5	500	50	-33996
Initial B3	0.00091	5	5495	500	0.5	-56726
Initial B4	0.00091	0.1	110	200	-0.23	-30964
Estimate B	**0.00154**	**0.625**	**409**	**349**	**0.303**	**-30472**
Initial C1	0.00091	0.1	110	600	3.42	-34627
Initial C2	0.01111	0.1	9	600	41.7	-35534
Initial C3	0.00091	2	2198	600	0.17	-35748
Initial C4	0.00091	0.1	110	200	-0.23	-30967
Estimate C	**0.00162**	**0.668**	**415**	**352**	**0.306**	**-30471**
True	**0.00200**	**0.500**	**250**	**300**	**0.300**	**-30470**

Table 3 : Simplex fitting estimates, varying λ_A, k_A and I_{re} (alternative dataset)

Vector	**λ_A**	**k_A**	**ρ_1**	**I_{re}**	**ρ_2**	**Log Likelihood**
Initial A1	0.00091	0	0	100	-	-35272
Initial A2	0.01832	0	0	100	-	-35160
Initial A3	0.00091	5	5495	100	-0.033	-57565
Initial A4	0.00091	0	0	500	-	-30560
Estimate A	**0.00145**	**0.517**	**358**	**455**	**0.477**	**-28958**
Initial B1	0.00091	0.1	110	500	1.056	-29897
Initial B2	0.01832	0.1	5.5	500	21.091	-30606
Initial B3	0.00091	5.0	5495	500	0.021	-57495
Initial B4	0.00091	0.1	110	200	1.68	-30394
Estimate B	**0.00177**	**0.482**	**273**	**407**	**0.452**	**-28951**
Initial C1	0.00091	0.1	110	600	1.967	-30886
Initial C2	0.01111	0.1	9	600	24.000	-31711
Initial C3	0.00091	2.0	2198	600	0.098	-40919
Initial C4	0.00091	0.1	110	200	1.68	-30377
Estimate C	**0.00164**	**0.505**	**308**	**434**	**0.487**	**-28956**
True	**0.00200**	**0.300**	**150**	**350**	**0.440**	**-28942**

Table 4 : Simplex fitting tested on model generated data

Dataset	λ_A	k_A	ρ_1	I_{re}	ρ_2	Mean Hz
set1 true	0.00130	0.40	308	330	0.37	5.49
set1 estimate	0.00135	0.55	406	369	0.38	5.56
set2 true	0.00220	0.35	159	170	0.09	2.77
set2 estimate	0.00137	0.32	233	178	0.10	2.81
set3 true	0.00110	0.45	409	220	0.14	3.24
set3 estimate	0.00134	0.64	462	229	0.14	3.28
set4 true	0.00170	0.80	471	350	0.32	5.11
set4 estimate	0.00157	0.78	496	367	0.34	5.15
set5 true	0.00240	0.37	154	380	0.55	7.43
set5 estimate	0.00189	0.47	249	437	0.57	7.50

Table 5 : Simplex fitting tested on recorded data, estimated fits

Dataset	λ_A	k_A	ρ_1	I_{re}	ρ_2	Mean Hz
mludw1	0.00134	0.372	277	335	0.35	5.79
mludw2	0.00155	0.756	487	370	0.34	4.80
t84_3	0.00216	0.331	153	168	0.08	2.39
t99_3	0.00111	0.401	359	218	0.14	3.50
t122_p2	0.00507	0.521	103	315	0.49	7.57